Journal of Solid State Chemistry 203 (2013) 326–332

Contents lists available at SciVerse ScienceDirect

Journal of Solid State Chemistry

journal homepage: www.elsevier.com/locate/jssc

Crystal structure of fluorite-related Ln_3SbO_7 (Ln=La–Dy) ceramics studied by synchrotron X-ray diffraction and Raman scattering

K.P.F. Siqueira [a], R.M. Borges [a], E. Granado [b], L.M. Malard [c], A.M. de Paula [c], R.L. Moreira [c], E.M. Bittar [d], A. Dias [a,*]

[a] Departamento de Química, Universidade Federal de Ouro Preto, Campus Morro do Cruzeiro, ICEB II, Ouro Preto—MG 35400-000, Brazil
[b] Instituto de Física "Gleb Wataghin", UNICAMP, Campinas—SP 13083-970, Brazil
[c] Departamento de Física, ICEx, Universidade Federal de Minas Gerais, C.P. 702, Belo Horizonte—MG 30123-970, Brazil
[d] Laboratório Nacional de Luz Síncrotron, C.P. 6192, 13083-970 Campinas, SP, Brazil

ARTICLE INFO

Article history:
Received 14 March 2013
Received in revised form
26 April 2013
Accepted 3 May 2013
Available online 13 May 2013

Keywords:
Synchrotron X-ray diffraction
SHG
Lanthanide
Antimonates
Raman scattering

ABSTRACT

Ln_3SbO_7 (Ln=La, Pr, Nd, Sm, Eu, Gd, Tb and Dy) ceramics were synthesized by solid-state reaction in optimized conditions of temperature and time to yield single-phase ceramics. The crystal structures of the obtained ceramics were investigated by synchrotron X-ray diffraction, second harmonic generation (SHG) and Raman scattering. All samples exhibited fluorite-type orthorhombic structures with different oxygen arrangements as a function of the ionic radius of the lanthanide metal. For ceramics with the largest ionic radii (La–Nd), the ceramics crystallized into the *Cmcm* space group, while the ceramics with intermediate and smallest ionic radii (Sm–Dy) exhibited a different crystal structure belonging to the same space group, described under the *Ccmm* setting. The results from SHG and Raman scattering confirmed these settings and ruled out any possibility for the non-centrosymmetric $C222_1$ space group describing the structure of the small ionic radii ceramics, solving a recent controversy in the literature. Besides, the Raman modes for all samples are reported for the first time, showing characteristic features for each group of samples.

1. Introduction

Ceramics of general formula Ln_3MO_7 (where Ln^{3+} is a lanthanide element and M is Os^{5+}, Re^{5+}, Ru^{5+}, Mo^{5+}, Ir^{5+}, Sb^{5+}, Nb^{5+} or Ta^{5+}) have been intensively studied because of their interesting photocatalytic activity [1], dielectric [2,3], and magnetic properties [4–7]. These materials present an ordered, defective fluorite-type structure, which was described by Hinatsu et al. [6], as follows: The unit cell for oxides has the general formula $M_4^{4+}O_8$, in which the four tetravalent metal ions are replaced by three trivalent ions (Ln) and one pentavalent ion (M), thus creating one oxygen vacancy per fluorite cell. Owing to the significant differences between the ionic radii of the Ln^{3+} and M^{5+}, cation ordering occurs on the metal sites and the oxide-vacancy orders on the anion sites.

A variety of crystal structures has been proposed for the Ln_3MO_7 ceramics, as a direct consequence of the great number of chemical combinations that is possible between the lanthanide ions and the element M (Ta, Nb, Sb, Mo) [1–7]. Also, the processing conditions can contribute to produce different crystallographic structures; for example, several polymorphic modifications can be achieved through temperature changes [5,6,8,9]. Since the physical properties are strictly dependent on the crystalline phase, it is important to determine the correct crystal structure for the produced ceramics before designing any possible application. The first structure determination for these ceramics was reported by Rossell [10], who proposed the *Cmcm* space group to describe the La_3NbO_7 crystal phase. However, the *Pnma* space group was later employed by Kahn-Harari et al. [11] to describe the crystal structure of this compound. In the literature, the *Cmcm* space group has been often used to describe the crystal structure of several members of the Ln_3MO_7 family: Ln_3RuO_7 (Ln=La–Eu) [6,12–15], Ln_3ReO_7 (Ln=Pr, Nd, Sm–Tb) [16,17], Ln_3OsO_7 (Ln=Pr, Nd, Sm–Gd) [18–20], Ln_3TaO_7 (Ln=La–Nd) [5,21], Ln_3IrO_7 (Ln=Pr, Nd, Sm, Eu) [9,22,23], Pr_3NbO_7 [21] and Ln_3SbO_7 (Ln=La–Nd) ceramics [6,7,21]. For Ln_3TaO_7 (Ln=Y, Sm–Ho) [5] and Ln_3MoO_7 (Ln=La–Nd, Sm, Eu) ceramics [24,25], the $C222_1$ and $P2_12_12_1$ space groups were previously described, respectively. Besides, the $Fm\bar{3}m$ space group was found for Ln_3TaO_7 (Ln=Ho–Lu) [5,6] and Ln_3NbO_7 (Ln=Dy–Lu) ceramics [4,6]. The $C222_1$ space group was also employed to describe the structure of Ln_3NbO_7 with intermediate

* Corresponding author.
E-mail addresses: anderson_dias@iceb.ufop.br, anderson_dias@ig.com.br (A. Dias).

0022-4596/$ - see front matter © 2013 Elsevier Inc. All rights reserved.
http://dx.doi.org/10.1016/j.jssc.2013.05.001

ionic radii *Ln* (*Ln*=Sm–Tb), while the *Pnma* space group was proposed for the larger ionic radii ceramics (*Ln*=La, Pr, Nd) [4]—in agreement with previous work by Kahn-Harari et al. [11].

Among all Ln_3MO_7 ceramics reported in the literature, a few studies have been carried out for *M*=Sb as pentavalent cation. In a pioneer work in the seventies, a series of Ln_3SbO_7 ceramics with *Ln*=Nd, Sm–Yb and Y were reported by Nath as belonging the pyrochlore ($Fd\bar{3}m$) structure [26]. Later on, Vente et al. proposed a fluorite related *Cmcm* group for Pr_3SbO_7 [21]. Then, Fennell et al. [27] proposed the $C222_1$ space group for Dy_3SbO_7 and Ho_3SbO_7. Recently, Hinatsu et al. [7] determined the *Cmcm* space group for *Ln*=La, Pr, Nd and $C222_1$ for *Ln*=Nd–Lu. However, Fu and Ijdo reported a critical, detailed study for all these structures and presented an alternative setting of the *Cmcm* space group, namely *Ccmm*, instead of $C222_1$, for Ln_3SbO_7 ceramics containing intermediate-sized lanthanides [28]. It can be concluded from this brief review that the proposed crystalline structures of Ln_3SbO_7 ceramics are still controversial. Concerning the conflicting structures reported in the literature, the description within the *Cmcm* space group has also been proposed for other Ln_3MO_7 ceramics by neutron diffraction [12,13,21], X-ray powder diffraction [4–7,9,17,18,28], as well as by X-ray single crystal diffraction [29]. In the case of the $C222_1$ space group, only studies using X-ray powder diffraction were reported [7].

In this context, the present paper intends to contribute to the elucidation of the possible crystal structure of Ln_3SbO_7 ceramics (*Ln*=La–Dy, exception of Ce and Pm), by reporting on our results of Raman scattering, second harmonic generation and synchrotron X-ray powder diffraction (SXRD). A similar methodology was previously applied by our group to solve structural conflicts for many materials [30–33].

2. Experimental

Ln_3SbO_7 ceramics were synthesized by using Ln_2O_3 (*Ln*=La, Nd, Sm, Eu, Gd, and Dy; >99.9% Sigma-Aldrich), Pr_6O_{11}, Tb_4O_7 (>99.9% Sigma-Aldrich) and Sb_2O_5 (>99.9% Sigma-Aldrich) as starting materials through solid-state reaction. All lanthanides used in this work were heat treated at 900 °C overnight before being employed for the synthesis. Stoichiometric amounts were weighed and mixed with a mortar and pestle. For the synthesis of La_3SbO_7 and Dy_3SbO_7 samples, an excess amount of about 200% weight of antimony oxide was added to ensure formation of Ln_3SbO_7 ceramics. For the synthesis of these ceramics, the conventional solid-state processing was employed in temperatures ranging from 1300 °C to 1500 °C, and times up to 15 h. After synthesis, diluted nitric acid (0.1 M) was employed to remove unreacted Gd_2O_3 and Tb_4O_7, which could be present in Gd_3SbO_7 and Tb_3SbO_7 ceramics, respectively. Then, the resulting products were washed in distilled water followed by drying at 80 °C.

SXRD measurements were taken in the superconducting wiggler XDS beamline of the Brazilian Synchrotron Laboratory, LNLS, with λ=0.65319 Å. The optical path of the beam upstream the sample position included a water-cooled Pt-coated vertically collimating mirror, a LN_2-cooled double Si(1 1 1) crystal monochromator with sagittal focusing and a Pt-coated vertically focusing mirror, yielding a highly monochromatic beam with dimensions of $2.0(H)\times 0.17(V)$ mm^2 full width at half maximum (FWHM) at the sample position. The samples were mounted in flat-plane $\theta/2\theta$ geometry with a spinning axis perpendicular to the sample surface to optimize grain statistics. The diffraction profiles were taken in the vertical scattering plane using a 0.3 mm slit located 0.80 m away from the sample followed by a highly-oriented pyrolitic graphite analyzer and a high-throughput $LaBr_3$ scintillator detector in the 2θ arm. This mounting resulted in high-resolution and low-background powder diffraction profiles, with typical Bragg peak widths of ~0.02° FWHM at low angles, and maximum peak heights of $\sim 10^5$ counts against a background level of $\sim 10^2$ counts. The measurements were performed in the range 4–90°2θ, covering ~2000 Bragg reflections, with a step size of 0.008°2θ. Rietveld refinements were performed using the GSAS+EXPGUI program [34].

Second harmonic generation (SHG) measurements were also performed. SHG is only present in structures lacking inversion symmetry [35], hence this technique can be used to determine the presence of this symmetry operation. We have used a 140 fs Ti–Sapphire oscillator (Coherent Chameleon) with 80 MHz repetition tuned at 800 nm which is directed to a modified Olympus FV300 scanning laser microscope. The backscattered signal is then directed to a dichroic mirror and a thin band pass centered at second harmonic wavelength (400 nm) to completely remove the laser scattered light where the SH signal is detect by a photomultiplier tube. We have used an alpha-quartz crystal with the laser incidence parallel to the *c*-axis as a reference for this measurement. The second harmonic emission from alpha-quartz is clearly detectable, although this material posses weak second order susceptibility (0.3 pm/V) compared to other materials [35].

Raman spectra of the as-synthesized samples were collected in backscattering configuration by using two different instruments. An Horiba LABRAM-HR spectrometer was used with the 632.8 nm line of a helium–neon laser as excitation source (effective power of 6 mW at the sample's surface), diffraction gratings of 600 and 1800 grooves/mm, Peltier-cooled charge coupled device (CCD) detector, confocal Olympus microscope (100 × objective), and experimental resolution typically 1 cm^{-1} for 10 accumulations of 30 s. Appropriate interference filter for rejecting laser plasma lines, and edge filters for stray light rejection were used. Also, a Horiba T64000 spectrometer (80 × objective) equipped with the 488 nm line of an Ar^+ laser (4 mW at the sample's surface) and a LN_2-cooled CCD detector was used. In this case, the spectral resolution was better than 2 cm^{-1} and the accumulation were equally 10 collections of 30 s. All resulting spectra were corrected by Bose–Einstein thermal factor [36].

3. Results and discussion

Representative SXRD profiles of Ln_3SbO_7 for *Ln*=La and Eu are given in Fig. 1(b) and (a), respectively. For the large-size lanthanides (*Ln*=La and Pr), a good agreement between observed and calculated diffraction data was obtained using a single orthorhombic phase within the *Cmcm* space group (see Fig. 1(b)), such as reported previously for these ceramics [10]. A relatively large deviation of the unit cell parameters (*a*, *b*, *c*) with respect to the idealized ($2a_c$,$\sqrt{2}a_c$,$\sqrt{2}a_c$) cell derived from the cubic fluorite structure (a_c~5.4 Å) was noticed. An alternative structural refinement for *Ln*=La under the *Pnma* space group with a distinct choice of axes ($a\sim\sqrt{2}a_c$,$b\sim 2a_c$,$c\sim\sqrt{2}a_c$), such as reported for La_3NbO_7 [11] was performed, also yielding a good fit to our diffraction data (χ^2=17.0 and 17.6 for refinements under *Cmcm* and *Pnma* space groups, respectively). However, the extra Bragg reflections expected for *Pnma* and forbidden by the higher symmetry *Cmcm* space group could not observed, indicating *Cmcm* is indeed the most suitable space group for Ln_3SbO_7 with *Ln*=La and Pr.

For medium size lanthanides, *Ln*=Sm–Dy, another crystalline phase with a much smaller orthorhombic distortion is observed (see Fig. 1(a) for *Ln*=Eu). Following previous studies, we attempted structural refinements for *Ln*=Eu using two possible space groups, $C222_1$ [7,27] and *Ccmm* [28], both with ($a\sim 2a_c$, $b\sim\sqrt{2}a_c$,$c\sim\sqrt{2}a_c$) metrics. Details regarding these two models can

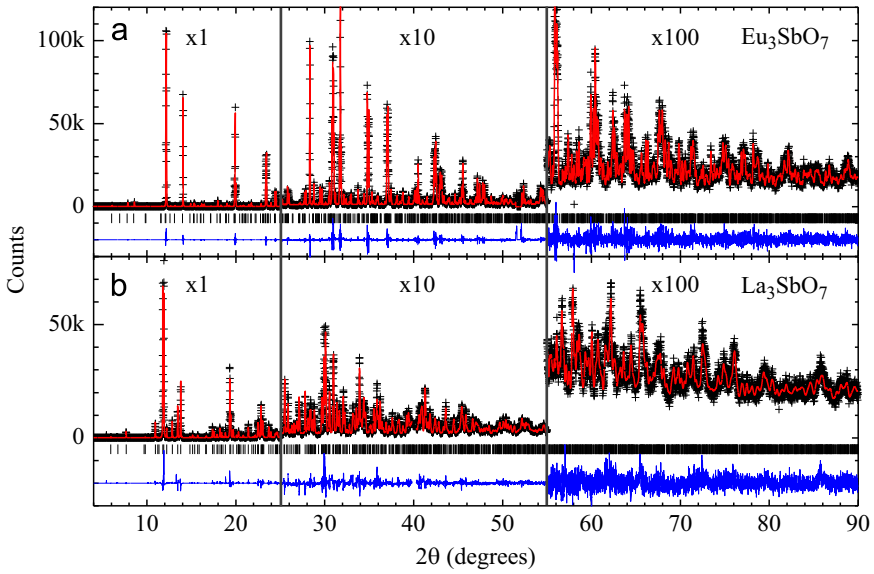

Fig. 1. SXRD patterns of Ln_3SbO_7 for (a) Ln=Eu and (b) Ln=La. The cross symbols and solid lines represent observed and calculated patterns, respectively. The difference curves are shown at the bottom of each figure. Vertical bars indicate the expected Bragg peak positions according to the crystal structure models described in the text and refined lattice parameters given in Fig. 2.

be found in Ref. [28]. The refinements under both space groups yielded equally good fits to the experimental data and nearly identical residuals [R_{wp}=9.94% and χ^2=6.80 for *Ccmm* and R_{wp}=9.89% and χ^2=6.73 for $C222_1$] supporting the proposition by Fu and Ijdo that the more symmetric *Ccmm* space group is most likely the correct one for the medium size lanthanides [28]. This conclusion is further supported by the absence of SHG signal (which indicates the existence of inversion symmetry center in the crystal structure) and by our Raman scattering (see discussion below). The structure of all the remaining samples with medium sized lanthanides was also successfully refined under the *Ccmm* space group. Although the *Ccmm* space group for Ln_3SbO_7 with medium-sized lanthanides is the same as the *Cmcm* used for the large sized lanthanides, the different settings were chosen to preserve the metrics of the unit cell in the complete series, with the longest orthorhombic axis along a ($a\sim2a_c$,$b\sim\sqrt{2}a_c$,$c\sim\sqrt{2}a_c$) [28].

We should mention that, despite presenting the same space group, the crystal structures for the large and medium/small lanthanides are distinct, with the SbO_6 octahedra being rotated around the long [1 0 0] direction for the *Cmcm* setting and [0 1 0] for the *Ccmm* setting [28], resulting in largely different diffraction profiles (see Fig. 1(a) and (b)). Finally, at the boundary between those structures, namely for Ln=Nd, both phases were identified in the diffraction profile and successfully refined, with weight fractions of 59% and 41% for the phases described under the *Cmcm* and *Ccmm* settings, respectively. Tables 1 and 2 present the refined structural parameters for Ln=La, Nd, Sm, Eu and Gd, after Rietveld analyses of SXRD data. The samples with Ln=Pr, Tb and Dy were also investigated, but the presence of unidentified minor impurities (other than unreacted oxides) prevented a reliable refinement of atomic positions and Debye–Waller parameters. For such samples, only the lattice parameters were extracted. Fig. 2 shows the evolution of the refined lattice parameters of Ln_3SbO_7 as a function of Ln^{3+} Shannon radii [38], summarizing the main findings of our SXRD analysis. The unit cell volumes show a discontinuous change from the phase described under the *Cmcm* setting to the one under *Ccmm*.

Vibrational studies are currently employed by our research group to investigate the behavior of the phonon modes for many electroceramic systems. Raman scattering besides theoretical factor-group analysis are powerful tools to obtain a complete set of reliable phonon modes, which in turn can help one determining the correct crystal structures. In this work, Raman scattering was used to confirm the results from SXRD and SHG techniques, aiming to show the relationship between crystal structure and vibrational modes, which allowed us to contribute to the debate on the crystalline structure of this class of ceramics. Raman spectra of Ln_3SbO_7 were collected at room-temperature, for all the produced ceramics. The results are displayed in Fig. 3 (two boards) for decreasing ionic radius (La–Dy). Because of strong electronic transitions that appear under certain conditions different laser lines were used. The final spectra showed in Fig. 3 represent the

Table 1
Refined structural parameters for Ln_3SbO_7 ceramics (Ln=La and Nd) with space group *Cmcm*. R_{wp} and R_p refer to background-subtracted values (Ref. [34]).

	La_3SbO_7	Nd_3SbO_7 phase I (59% w.f.)
a (Å)	11.1495(3)	10.8870(2)
b (Å)	7.6356(2)	7.52218(11)
c (Å)	7.7477(2)	7.63180(11)
*Ln*1 (0,0,0)		
B (Å^2)	0.62(3)	0.73(3)
*Ln*2 (x,y,1/4)		
X	0.22727(9)	0.22858(8)
Y	0.29716(12)	0.29188(10)
B (Å^2)	0.47(2)	0.47(2)
Sb (0,1/2,0)		
B (Å^2)	0.51(3)	0.59(3)
O1 (x,y,z)		
X	0.1283(7)	0.1270(8)
Y	0.3157(10)	0.3155(9)
z	−0.0348(10)	−0.0326(9)
O2 (x,y,1/4)		
x	0.1207(10)	0.1278(11)
y	0.0219(15)	0.0205(13)
O3 (0,y,1/4)		
y	0.442(2)	0.428(2)
B-oxygen (Å^2)	0.78(12)	0.69(12)
R_{wp}/R_p (%)	18.2/12.9	11.0/8.4
χ^2	17.0	7.0

Table 2
Refined structural parameters for Ln_3SbO_7 (Ln=Nd, Sm, Eu and Gd) with space group *Ccmm*. R_{wp} and R_p refer to background-subtracted values (Ref. [34]).

	Nd_3SbO_7 phase II (41% w.f.)	Sm_3SbO_7	Eu_3SbO_7	Gd_3SbO_7
a (Å)	10.8436(2)	10.72269(11)	10.67411(10)	10.62843(7)
b (Å)	7.62229(14)	7.55640(7)	7.52595(7)	7.51729(5)
c (Å)	7.67228(13)	7.60704(7)	7.57999(7)	7.54486(5)
*Ln*1 (0,1/2,0)				
B (Å^2)	0.32(4)	0.49(2)	0.53(2)	0.49(3)
*Ln*2 (*x*,*y*,1/4)				
X	0.23461(10)	0.23484(6)	0.23470(5)	0.23406(7)
Y	0.2364(2)	0.23525(8)	0.23500(6)	0.23453(11)
B (Å^2)	0.35(3)	0.46(1)	0.41(1)	0.34(1)
Sb (0,0,0)				
B (Å^2)	0.43(5)	0.44(2)	0.32(2)	0.32(2)
O1 (*x*,*y*,*z*)				
X	0.1332(13)	0.1254(6)	0.1243(5)	0.1232(9)
Y	0.1893(15)	0.1934(8)	0.1934(7)	0.1967(12)
Z	−0.0264(12)	−0.0269(7)	−0.0280(7)	−0.0349(12)
O2 (*x*,0,1/4)				
X	0.054(2)	0.0551(12)	0.0651(11)	0.056(2)
O3 (*x*,1/2,1/4)				
X	0.121(3)	0.1212(12)	0.1271(10)	0.127(2)
O4 (*x*,1/2,1/4)				
X	−0.126(3)	−0.1296(13)	−0.1336(10)	−0.140(2)
B-oxygen (Å^2)	0.9(2)	0.52(8)	1.3(2)	0.6(2)
R_{wp}/R_p (%)	11.0/8.4	10.9/7.1	9.9/7.4	20.3/10.1
χ^2	7.0	8.6	6.8	20.6

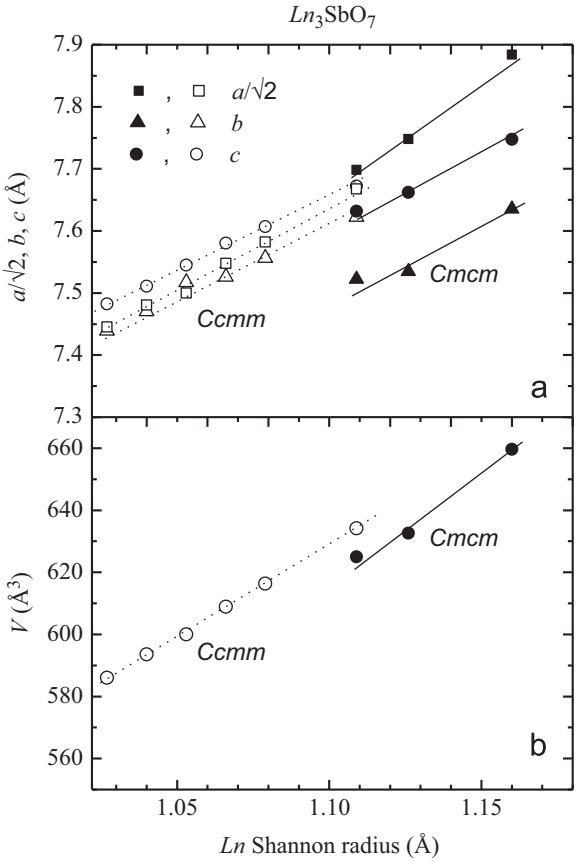

Fig. 2. (a) Lattice parameters $a/\sqrt{2}$, *b*, and *c*, and (b) unit cell volumes of Ln_3SbO_7 as a function of *Ln* Shannon radius (coordination number, *CN*=8), for the distinct crystal phases observed in the series. Statistical error bars are smaller than the symbol sizes.

best obtained results using an excitation blue line (488 nm) for Gd, and a red line (632.8 nm) for La, Pr, Nd, Sm, Eu, Tb and Dy.

Aiming to understand and discuss the results from Raman scattering, group-theory calculations for the main structures related to Ln_3SbO_7 ceramics are now presented. Table 3 shows Wyckoff positions and phonons distribution at the Brillouin zone center in terms of the irreducible representations, according to the method developed by Rousseau et al. [37] for the Ln_3SbO_7 crystal structures within the *Cmcm*, *Ccmm* and $C222_1$ space groups. As it can be seen, 27 Raman-active modes are expected in the *Cmcm* space group, as well as in its alternative *Ccmm* setting. The differences between the group-theory predictions for these two structures come from the different oxygen occupations. In the structure for large size *Ln*, described by the *Cmcm* setting, oxygen atoms occupy 4*c*, 16*h* and 8*g* sites. However, in the *Ccmm* structure, there are four distinct oxygen ions: O(1) occupies a 16*h* site, while the others O(2)–O(4) occupy 4*c* sites. Thus, the site group method of Rousseau et al. [37] leads to the following distribution of the phonon modes at the Brillouin zone center: $8A_g+8B_{1g}+5B_{2g}+6B_{3g}$ for *Cmcm*, and $8A_g+8B_{1g}+4B_{2g}+7B_{3g}$ for *Ccmm*. The other possibility for the crystalline structures of Ln_3SbO_7, as proposed by previous authors and not excluded by our X-ray diffraction analysis for medium sized *Ln*, would be the non-centrosymmetric $C222_1$ space group. In this case, excluding the acoustic modes, 63 bands are expected in the Raman spectra for this structure ($14A+18B_1+16B_2+15B_3$).

For all samples, a careful analysis was carried out by fitting the Raman experimental data with Lorentzian curves. The results are presented in Fig. 4 for La_3SbO_7 and Eu_3SbO_7. This procedure revealed 23 modes for the La, and 24 Raman bands for the Eu ceramics, respectively. As a general trend, the phonon wavenumbers down-shifted, as a consequence of the decreasing tendency of the ionic radii (see also Fig. 3 for a better visualization of this general trend and the discussion below). We cannot visualize all the 27 bands because some of them could occur at very low frequencies (below 70 cm^{-1}) and others could be relatively weak to be discerned. As a whole, we could see a total of 25 Raman-active bands. These results are in agreement with the predictions for the *Cmcm* and *Ccmm* groups (Table 3). Also, the Raman patterns show that Ln_3SbO_7 ceramics do not show the large number of modes expected for the structure described by the $C222_1$ space group, providing further evidence against a description of the crystal structure of these ceramics under this space group.

Although the materials described under the *Cmcm* and *Ccmm* settings exhibited an equal number of Raman-active modes, they present some peculiarities in their Raman patterns. Fig. 5 shows two different regions of the spectra, where these peculiarities can be clearly seen. In Fig. 5(a) we can observe that the bands around 170 cm^{-1} and 187 cm^{-1} are well-defined for the La and Pr, up-shifting and overlapping for smaller lanthanides. This change of behavior begins exactly for the sample containing Nd, which presents a mixture of the two distinct orthorhombic phases (see above). Likewise, the bands around 440 cm^{-1} can be considered as fingerprint of the structure described under *Ccmm*, which presents a larger number of active modes in this region than the structure described under *Cmcm*, as shown in Fig. 5(b). Then, by analyzing the results from Raman scattering, we can discern between these two orthorhombic structures. In this way, this method provides a powerful tool for determining the crystal structure

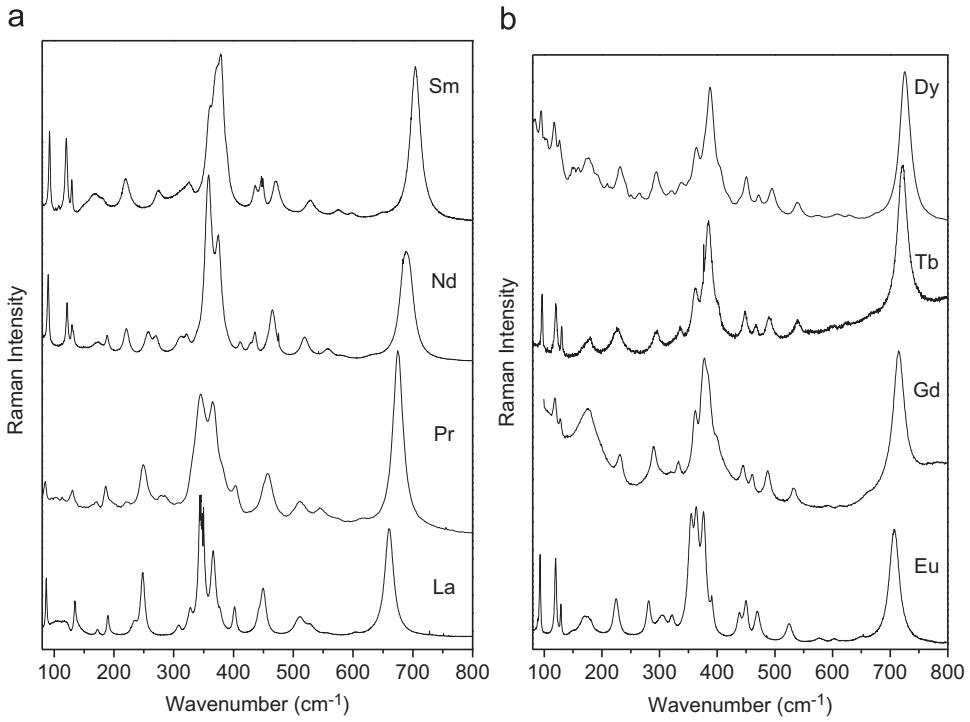

Fig. 3. Room-temperature Raman spectra for all Ln_3SbO_7 ceramics. The sequence plotted reproduces the variation (decreasing tendency) in the ionic radius (a) La–Sm; (b) Eu–Dy.

of ternary oxides, along with XRD. Concerning the second phase that is present in samples with smaller ionic radius such as observed by XRD, no extra Raman band was observed, indicating that either this extra phase presents a high-symmetry structure with little or no Raman activity, or the separation between the phonon bands for these structures are significantly smaller than the corresponding band widths.

A final analysis of the Raman modes for all Ln_3SbO_7 ceramic samples could be accomplished after their adjustment by Lorentzian lines. Due to the proximity between the two structures assumed by the ceramics along the La–Dy series, we could correlate the behavior of the phonon modes, despite the structural change presented. It is clear from Figs. 3–5 that different tendencies can be verified for increasing ionic radii. For the majority of the modes, the wavenumbers increased for decreasing ionic radii (Figs. 3–5), as expected [39]. This behavior is due to the phenomenon of lanthanide contraction, where the cell volume decreases in lanthanides with higher atomic numbers. Moreover, it was verified that the modes assumed distinct regimes between the two orthorhombic phases, which indicates that this phenomenon acts differently, as a function of the actual crystal structure (*Ccmm* or *Cmcm*).

Table 3
Factor-group analysis for crystal structures previously reported by the literature for the Ln_3SbO_7 ceramics.

Ion	Wyckoff sites	Symmetry	Irreducible representations
Orthorhombic (*Cmcm*, #63)			
$Ln^{+3}(1)$	4*a*	C_{2h}^{x}	No Raman-active mode
$Ln^{+3}(2)$	8*g*	C_{s}^{xy}	$2A_g+2B_{1g}+B_{2g}+B_{3g}$
Sb^{+5}	4*b*	C_{2h}^{x}	No Raman-active mode
$O^{-2}(1)$	4*c*	C_{2h}^{y}	$A_g+B_{1g}+B_{3g}$
$O^{-2}(2)$	16*h*	C_1	$3A_g+3B_{1g}+3B_{2g}+3B_{3g}$
$O^{-2}(3)$	8*g*	C_{s}^{xy}	$2A_g+2B_{1g}+B_{2g}+B_{3g}$
$\Gamma_{RAMAN}=8A_g+8B_{1g}+5B_{2g}+6B_{3g}$			
Orthorhombic (*Ccmm*, #63)			
$Ln^{+3}(1)$	4*b*	C_{2h}^{x}	No Raman-active mode
$Ln^{+3}(2)$	8*g*	C_{s}^{xy}	$2A_g+2B_{1\,g}+B_{2\,g}+B_{3\,g}$
Sb^{+5}	4*a*	C_{2h}^{x}	No Raman-active mode
$O^{-2}(1)$	16*h*	C_1	$3A_g+3B_{1g}+3B_{2g}+3B_{3g}$
$O^{-2}(2)$	4*c*	C_{2h}^{y}	$A_g+B_{1g}+B_{3g}$
$O^{-2}(3)$	4*c*	C_{2h}^{y}	$A_g+B_{1g}+B_{3g}$
$O^{-2}(4)$	4*c*	C_{2h}^{y}	$A_g+B_{1g}+B_{3g}$
$\Gamma_{RAMAN}=8A_g+8B_{1g}+4B_{2g}+7B_{3g}$			
Orthorhombic ($C222_1$, #20)			
$Ln^{+3}(1)$	4*b*	C_2^{y}	$A+2B_1+B_2+2B_3$
$Ln^{+3}(2)$	8*c*	C_1	$3A+3B_1+3B_2+3B_3$
Nb^{+5}	4*b*	C_2^{y}	$A+2B_1+B_2+2B_3$
$O^{-2}(1)$	8*c*	C_1	$3A+3B_1+3B_2+3B_3$
$O^{-2}(2)$	8*c*	C_1	$3A+3B_1+3B_2+3B_3$
$O^{-2}(3)$	4*a*	C_2^{x}	$A+2B_1+2B_2+B_3$
$O^{-2}(4)$	4*a*	C_2^{x}	$A+2B_1+2B_2+B_3$
$O^{-2}(5)$	4*a*	C_2^{x}	$A+2B_1+2B_2+B_3$
$\Gamma_{RAMAN}=14A+18B_1+16B_2+15B_3$ (once $\Gamma_{Acoustic}=B_1+B_2+B_3$)			

4. Conclusions

Ln_3SbO_7 (Ln=La, Pr, Nd, Sm, Eu, Gd, Tb and Dy) ceramics were synthesized in optimized conditions of temperature and time. The produced ceramics were investigated by SXRD, SHG and Raman scattering. All the samples exhibited orthorhombic superstructures of the cubic fluorite-type, but with different arrangements as a function of the ionic radius of the lanthanide metal. La_3SbO_7 and Pr_3SbO_7 ceramics crystallized in a structure described by the space group *Cmcm*, while the other ceramics (Sm–Dy) exhibited a distinct crystal structure described under an alternative setting of the same space group, *Ccmm*. Nd_3SbO_7 presents roughly an equal mixture of these two phases. The overall results allowed us to discuss on the controversies pointed out by the literature concerning the crystal structure of these ceramics. The setting for the space group *Ccmm* instead of the

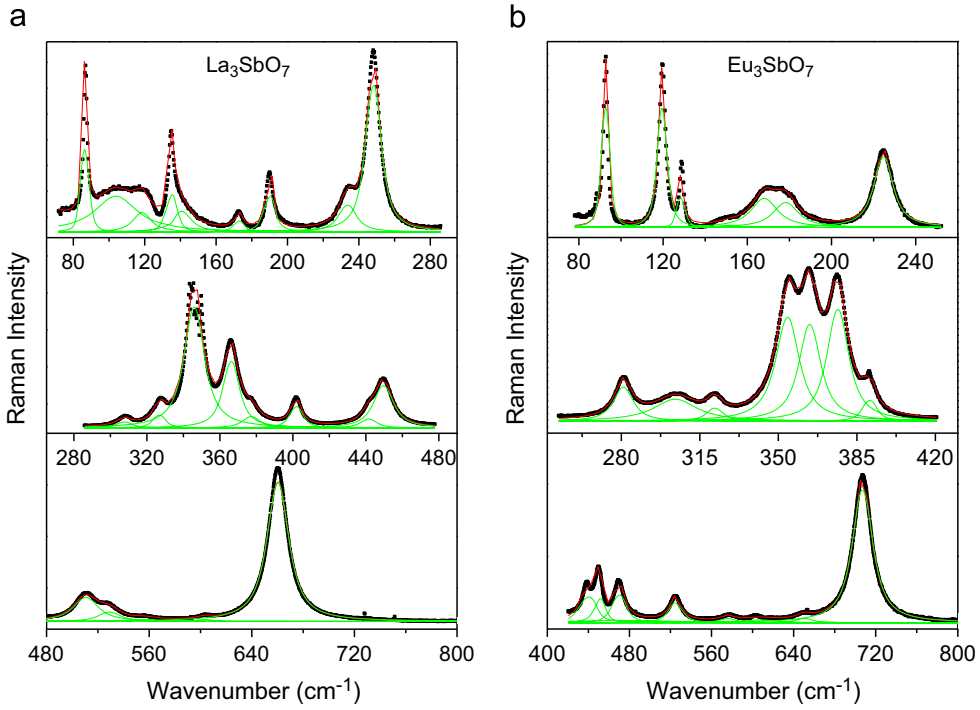

Fig. 4. Micro-Raman spectra of the orthorhombic structures: (a) La_3SbO_7 (*Cmcm* space group), and (b) Eu_3SbO_7 (*Ccmm* space group). Experimental data are in closed squares, whereas the fitting curves are represented by red lines. Green lines represent the phonon modes adjusted by Lorentzian curves. The Raman spectra were divided in three regions for better visualization. (For interpretation of the references to color in this figure legend, the reader is referred to the web version of this article.)

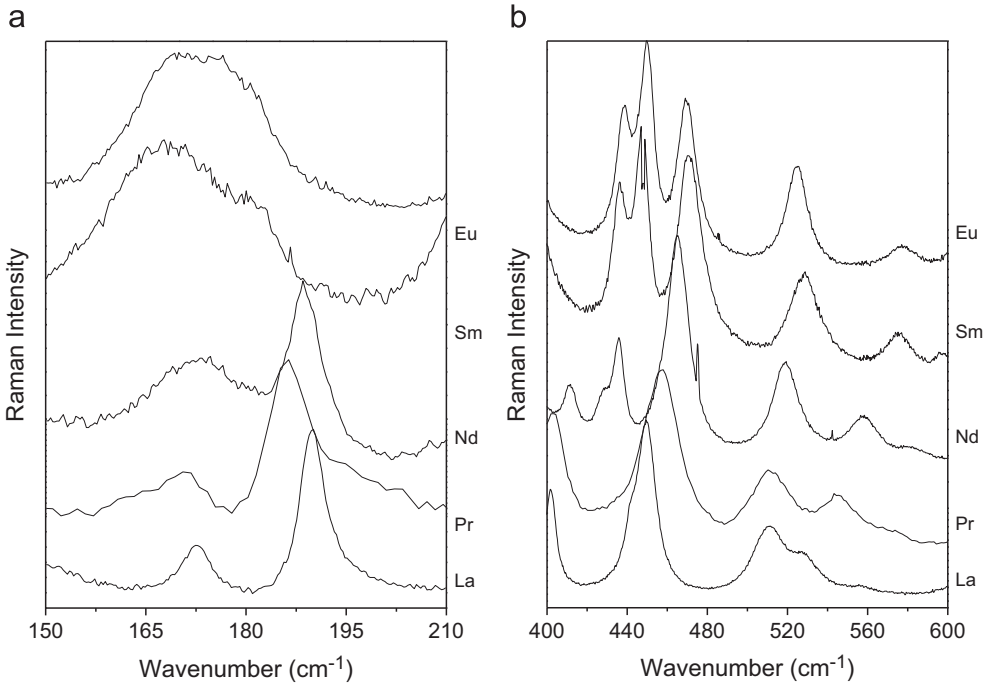

Fig. 5. Raman spectra (zoom) for the samples containing La, Pr, Nd, Sm and Eu: (a) 150–210 cm^{-1}; (b) 400–600 cm^{-1}. Peculiarities in the Raman patterns between *Cmcm* and *Ccmm* structures can be visualized in these regions.

less symmetrical space group $C222_1$ is more appropriate for these ceramics, because of the absence of SHG signals and the large difference between the vibrational modes observed experimentally and those predicted by group-theory calculations for each space group. The results from Raman spectroscopy are in perfect agreement with theoretical calculations and corroborate the results from SXRD and SHG.

Acknowledgments

The authors acknowledge the financial support from CAPES, CNPq, FINEP and FAPEMIG. Special thanks to Dr. Cristiano Fantini Leite and Prof. Marcos A. Pimenta (UFMG) for their hospitality during Raman experiments with the T64000 equipment. LNLS is acknowledged for concession of beamtime.

References

[1] R. Abe, M. Higashi, Z.G. Zou, K. Sayama, Y. Abe, H. Arakawa, J. Phys. Chem. B 108 (2004) 811–814.
[2] L. Cai, J.C. Nino, J. Eur. Ceram. Soc. 27 (2007) 3971–3976.
[3] L. Cai, J.C. Nino, J. Eur. Ceram. Soc. 30 (2010) 307–313.
[4] Y. Doi, Y. Harada, Y. Hinatsu, J. Solid State Chem. 182 (2009) 709–715.
[5] M. Wakeshima, H. Nishimine, Y. Hinatsu, J. Phys. Condens. Matter 16 (2004) 4103–4120.
[6] M. Wakeshima, Y. Hinatsu, J. Solid State Chem. 183 (2010) 2681–2688.
[7] Y. Hinatsu, H. Ebisawa, Y. Doi, J. Solid State Chem. 182 (2009) 1694–1699.
[8] L. Cai, S. Denev, V. Gopalan, J.C. Nino, J. Am. Ceram. Soc. 93 (2010) 875–880.
[9] Y. Hinatsu, Y. Doi, H. Nishimine, M. Wakeshima, M. Sato, J. Alloys Compd. 488 (2009) 541–545.
[10] H.J. Rossell, J. Solid State Chem. 27 (1979) 115–122.
[11] A. Kahn-Harari, L. Mazerolles, D. Michel, F. Robert, J. Solid State Chem. 116 (1995) 103–106.
[12] P. Khalifah, Q. Huang, J.W. Lynn, R.W. Erwin, R.J. Cava, Mater. Res. Bull. 35 (2000) 1–7.
[13] F. Wiss, N.P. Raju, A.S. Wills, J.E. Greedan, Int. J. Inorg. Mater. 2 (2000) 53–59.
[14] D. Harada, Y. Hinatsu, Y. Ishii, J. Phys. Condens. Matter 13 (2001) 10825–10836.
[15] D. Harada, Y. Hinatsu, J. Solid State Chem. 158 (2001) 245–253.
[16] R. Lam, T. Langet, J.E. Greedan, J. Solid State Chem. 171 (2002) 317–323.
[17] Y. Hinatsu, M. Wakeshima, N. Kawabuchi, N. Taira, J. Alloys Compd. 374 (2004) 79–83.
[18] J.R. Plaisier, R.J. Drost, D.J.W. IJdo, J. Solid State Chem. 169 (2002) 189–198.
[19] W.R. Gemmill, M.D. Smith, Y.A. Mozharivsky, G.J. Miller, H.-C. zur Loye, Inorg. Chem. 44 (2005) 7047–7055.
[20] R. Lam, F. Wiss, J.E. Greedan, J. Solid State Chem. 167 (2002) 182–187.
[21] J.F. Vente, R.B. Helmholdt, D.J.W. IJdo, J. Solid State Chem. 108 (1994) 18–23.
[22] J.F. Vente, D.J.W. IJdo, Mater. Res. Bull. 26 (1991) 1255–1262.
[23] H. Nishimine, M. Wakeshima, Y. Hinatsu, J. Solid State Chem. 177 (2004) 739–744.
[24] J.E. Greedan, N.P. Raju, A. Wegner, P. Gougeon, J. Padiou, J. Solid State Chem. 129 (1997) 320–327.
[25] H. Nishimine, M. Wakeshima, Y. Hinatsu, J. Solid State Chem. 178 (2005) 1221–1229.
[26] D.K. Nath, Inorg. Chem. 9 (1970) 2714–2718.
[27] T. Fennell, S.T. Bramwell, M.A. Green, Can. J. Phys. 79 (2001) 1415–1419.
[28] W.T. Fu, D.J.W. IJdo, J. Solid State Chem. 182 (2009) 2451–2455.
[29] W.R. Gemmill, M.D. Smith, H.-C. zur Loye, Inorg. Chem. 43 (2004) 4254–4261.
[30] R.L. Moreira, R.P.S.M. Lobo, G. Subodh, M.T. Sebastian, F.M. Matinaga, A. Dias, Chem. Mater. 19 (2007) 6548–6554.
[31] A. Dias, R.G. Sá, R.L. Moreira, J. Raman Spectrosc. 39 (2008) 1805–1810.
[32] A. Dias, K.P.F. Siqueira, J. Raman Spectrosc. 41 (2010) 93–97.
[33] A. Dias, G. Subodh, M.T. Sebastian, R.L. Moreira, J. Raman Spectrosc. 41 (2010) 702–706.
[34] A.C. Larson,R.B. Von Dreele, Los Alamos National Laboratory Report LAUR 86-748, 2000;
B.H. Toby, J. Appl. Crystallogr. 34 (2001) 210–213.
[35] R.W. Boyd, Non Linear Optics, third ed., Academic Press, Burlington, MA, 2008.
[36] W. Hayes, R. Loudon, Scattering of Light by Crystals, Wiley, New York, 1978.
[37] D.L. Rousseau, R.P. Bauman, S.P.S. Porto, J. Raman Spectrosc. 10 (1981) 253–290.
[38] R.D. Shannon, Acta Crystallogr. Sect. A: Found. Crystallogr. 32 (1976) 751–767.
[39] K.F.P. Siqueira, R.L. Moreira, A. Dias, Chem. Mater. 22 (2010) 2668–2674.